Density Matrix Based Transport in Heterostructure Devices Utilizing Tight-Binding Approaches

1st Mathias Pech
Chair for Communication Technology
TU Dortmund
Dortmund, Germany
mathias.pech@tu-dortmund.de

2nd Alan Abdi
Chair for Communication Technology
TU Dortmund
Dortmund, Germany
alan.abdi@tu-dortmund.de

3rd Dirk Schulz
Chair for Communication Technology
TU Dortmund
Dortmund, Germany
dirk2.schulz@tu-dortmund.de

2024 International Conference on Simulation of Semiconductor Processes and Devices (SISPAD) | 979-8-3315-1635-2/24/$31.00 ©2024 IEEE | DOI: 10.1109/SISPAD62626.2024.10732994

Abstract—By combining a tight-binding solid-state description with an equation of motion for a density matrix defined at the same lattice points, an efficient and atomistic transport model emerges. Instead of mapping the density matrix onto a phase space function like the Wigner function we maintain a real space description, allowing for easy implementation of spatially varying lattice distances and hopping terms. This vastly extends the possible applications of density matrix approaches which on one hand usually require a constant discretization width to perform a Fourier transform and on the other hand usually start from a simple effective mass Hamiltonian. Our approach is applied onto GaAs/Al_xGa_{1-x}As resonant tunneling diodes and agrees well with stationary results obtained by a quantum transmitting boundary method. The explicit time-resolved algorithm is shown to converge well and shows great computational efficiency when compared to a Quantum Liouville-type equation. Additionally, the derived equation of motion is well suited for the extension to more complex problems, especially tight binding models that take more neighbors or different orbitals into account.

Index Terms—Computational nanotechnology, Quantum transport, von-Neumann equation, Density Matrix, Heterostructures

I. Introduction

Even though the interest and research into density matrix approaches and foremost the Wigner transport equation (WTE) remains strong [1], they still have not caught up to the standard of other transport models, where the options to include for example multiple band tight-binding models or even first-principles methods are readily available and easily solved in real or mode-space (e.g. [2], [3]). However, on account of the extreme computational burden these methods are mostly restricted to the stationary case. In order to fill the gap of quantum transport models capable to model the atomistic yet time-resolved device behavior in e.g. THz amplifiers or ultrafast switches an equation of motion for the density matrix based on a tight-binding Hamiltonian can be set up. Here, we extend our previously presented approach for such equation [4], [5] in two major ways. Most importantly, the density matrix is solved in real space and on a staggered grid that results from the tight-binding Hamiltonian. In addition, it is applied onto a GaAs/Al_xGa_{1-x}As resonant tunneling diode (RTD) (Fig. 1a) with the inclusion of spatially varying hopping terms, corresponding to a spatially dependent effective mass in the usual models. Two different values for the alloy content $x = 0.2$ and $x = 0.3$ are considered which lead to different strength of the discontinuity at the GaAs/AlGaAs interfaces. For the sake of simplicity, a replacement model with only the nearest neighbor interaction taken into account is used.

II. Equation of motion for the tight-binding density matrix

The derivation of the equation of motion for the tight-binding density matrix is summarized briefly, as it mainly follows [4] where, however, the resulting transport equation was mapped onto phase space and simplified to a uniform grid formulation. To start off, the tight-binding Hamiltonian for a one-dimensional atomic chain with the atoms located at the locations u is expressed in terms of fermionic creation and annihilation operators $\hat{c}^\dagger$ and $\hat{c}$

$$\hat{H} = \sum_{u,m} \hat{\gamma}_{um} \hat{c}_u^\dagger \hat{c}_m + \sum_u \epsilon_u \hat{c}_u^\dagger \hat{c}_u, \tag{1}$$

where $\hat{\gamma}_{um}$ contains the hopping energy to the atom at lattice location m and ϵ_u the onsite energy [6]. Similarly, the density operator can be written in terms of the fermionic field operators

$$\hat{\rho} = \sum_j \varphi_j^*(\boldsymbol{r}) \hat{c}_j^\dagger \cdot \sum_i \varphi_i(\boldsymbol{r'}) \hat{c}_i, \tag{2}$$

with the orbital functions contained in φ_i and φ_j. After multiplying (2) with φ_l from the left and φ_s^* from the right and integrating over $\boldsymbol{r}$ and $\boldsymbol{r'}$, the density operator at the lattice site ls is given by the pair operator [4]

$$\hat{\rho}_{ls} = \hat{c}_l^\dagger \hat{c}_s. \tag{3}$$

Here, the coordinates l and s correspond to the conventional coordinates x and x'. Inserting (1) and (3) into a Heisenberg equation of motion and utilizing fermionic commutator rules leads to an equation for the density matrix elements defined in terms of the expectation value of the pair operator [7] $\rho_{ls} = \langle \hat{\rho}_{ls} \rangle$:

$$-\imath\hbar \frac{d}{dt} \rho_{ls} = \sum_u \gamma_{ul} \rho_{us} - \sum_m \gamma_{ms} \rho_{lm} + (\epsilon_l - \epsilon_s) \rho_{ls}, \tag{4}$$

as is visualized in Fig. 1b. Similar to the coordinate transform in the Wigner-Weyl transform, the coordinates l and s are then mapped onto the discrete center of mass coordinates χ and ξ according to

$$\chi = \frac{(l+s)}{2} \quad \text{and} \quad \xi = l - s, \tag{5}$$

resulting in a nonuniform grid of locations for the tight-binding density matrix in center of mass coordinates.

If a constant lattice spacing for the initial tight-binding Hamiltonian is assumed, the density matrix elements can be expressed in terms of the vectors $\boldsymbol{p}_n = \boldsymbol{p}(\chi_n, \xi_{r=1}, ..., \xi_{r=N_\xi})$ and $\boldsymbol{q}_{n+\frac{1}{2}} = \boldsymbol{q}(\chi_{n+\frac{1}{2}}, \xi_{r=\frac{3}{2}}, ..., \xi_{r=N_\xi-\frac{1}{2}})$, which form a staggered grid with an alternating even and odd number of ξ elements (see Fig. 1c). In this regard the presented approach is not unlike the method originally investigated by Mains and Haddad by a rigorous derivation of the Wigner function [8], albeit in real space and not phase space.

Rewriting (4) in center of mass coordinates and in matrix and vector notation yields the two coupled equations

$$\begin{aligned} -\imath\hbar\frac{\partial}{\partial t}\boldsymbol{p}_n &= \boldsymbol{M}_{n-\frac{1}{2}} \cdot \boldsymbol{q}_{n-\frac{1}{2}} - \boldsymbol{M}_{n+\frac{1}{2}} \cdot \boldsymbol{q}_{n+\frac{1}{2}} + \boldsymbol{V}_n \cdot \boldsymbol{p}_n \\ -\imath\hbar\frac{\partial}{\partial t}\boldsymbol{q}_{n+\frac{1}{2}} &= \boldsymbol{M}_n \cdot \boldsymbol{p}_n - \boldsymbol{M}_{n+1} \cdot \boldsymbol{p}_{n+1} + \boldsymbol{V}_{n+\frac{1}{2}} \cdot \boldsymbol{q}_{n+\frac{1}{2}} \end{aligned} \tag{6}$$

with the matrix

$$\boldsymbol{M}_{n-\frac{1}{2}} = \begin{bmatrix} \gamma_{(n-\frac{1}{2},r=1),(n,r=\frac{3}{2})} & 0 & 0 & 0 \\ -\gamma_{(n-\frac{1}{2},r=2),(n,r=\frac{3}{2})} & \gamma_{(n-\frac{1}{2},r=2),(n,r=\frac{5}{2})} & 0 & 0 \\ 0 & -\gamma_{...} & \gamma_{...} & 0 \\ 0 & 0 & -\gamma_{...} & \ddots \end{bmatrix} \tag{7}$$

containing the hopping terms and the diagonal matrix $\boldsymbol{V}_n$ which contains the matrix elements $V_{n,r} = \epsilon_{n+\frac{1}{2}r} - \epsilon_{n-\frac{1}{2}r} + \bar{V}_{n+\frac{1}{2}r} - \bar{V}_{n+\frac{1}{2}r}$ on its diagonal that include the onsite energies ϵ and any applied external biases $\bar{V}$. The expressions for $\boldsymbol{M}_n$ and $\boldsymbol{V}_{n+\frac{1}{2}}$ are similar and thus omitted. Only the nearest neighbor coupling is included in (6) for the sake of simplicity. However, the extension to account for more neighbors is straightforward [4]. (6) is the basis for all further stationary and transient studies.

A. Discussion of the proposed approach

The key aspects of the resulting formalism are summarized in the following section. In contrast to most other density matrix approaches in literature, most notably those utilizing the WTE, no information is lost during the transform onto center of mass coordinates [8], [9]. This is because no unitary transform between the coordinates is possible, if a uniform discretization grid is used in both the original and the center mass of mass coordinates. This is alleviated by the use of a staggered grid, though the domain of the two descriptions still does not coincide exactly because of the system

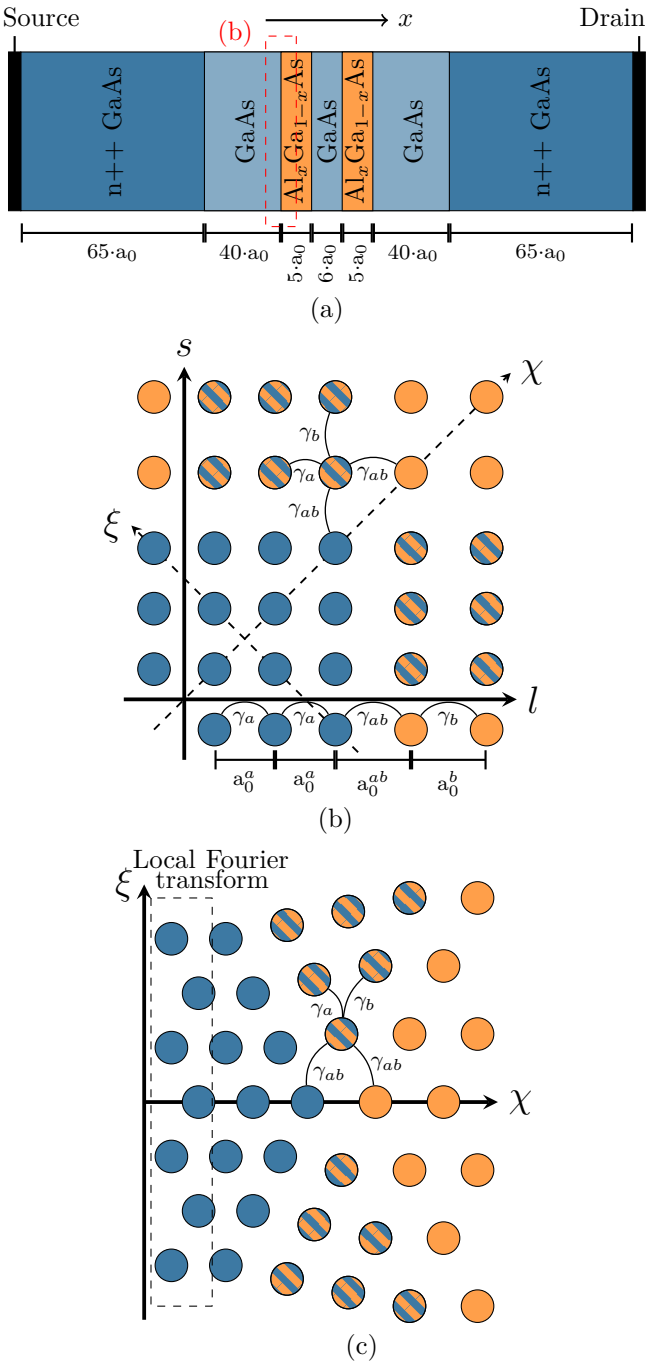

Fig. 1. A schematic of the resonant tunneling diode is shown (a) along with the consequent tight-binding density matrix scheme (b) for an atomic chain of the materials a (e.g. GaAs) and b (e.g AlGaAs). The resulting locations of the density matrix elements in center of mass coordinates are shown in (c). For the device in question the difference in lattice spacing is vastly exaggerated for the sake of clarity, as the lattice constants of GaAs and AlGaAs differ by less than 0.1 %.

boundaries [9]. Additionally, there is no need to introduce discretization schemes such as upwind or finite volume methods in the first place, as the discretization directly follows from the tight-binding Hamiltonian and locations of the replacement orbitals that are used. Another benefit

lies in the fact, that a spatially varying lattice spacing in heterostructures can readily be taken into account, as long as the contacts are sufficiently long and the lattice spacing in the drain and source contacts is constant since the Fourier transform is only applied locally at the device contacts to include inflow boundary conditions [10], as it can also be seen from Fig. 1c. Finally, the real space system matrix exhibits far higher sparsity than its phase space counterparts and can thus, when combined with the application of an explicit Runge-Kutta method for the time derivative, lead to lower computation times and lower memory requirements. In the case of spatially varying hopping terms (i.e. spatially varying effective masses) first results show that transient simulations run on the same hardware (Intel Xeon E5) are more than one order of magnitude faster when compared to a Quantum Liouville-type equation (QLTE) with typical discretization values (see [11]), though further quantitative research regarding the relative error is necessary.

However, these advantages come with several new challenges when the algorithm is applied, especially onto open devices such as RTDs or FETs. First and foremost, the boundary conditions in χ and ξ have a large impact on the numerical stability. In terms of the inflow boundary conditions, these issues arise as part of the discretization pattern shown in (6). Whereas for conventional methods only one boundary term per contact is needed, with the proposed method two inflow boundary terms are set up, e.g. in case of the drain contact $\boldsymbol{p}_1$ and $\boldsymbol{q}_{\frac{3}{2}}$ in order for the system matrix to have a full rank. As such, inflow boundary conditions are needed for density matrix elements which do not lie at the device contacts and therefore do not necessarily obey the Fermi distribution. This issue can be alleviated by introducing long contact regions with a constant potential. Further research of the influence of the complex absorbing potential (CAP) [12] on the staggered grid density matrix formalism is also needed. Compared to the conventional applications of the WTE or QLTE (e.g. [11]) even small deviations of the CAP parameters such as amplitude or length influence the obtained charge carrier density, so that e.g. analysis of the eigenvalue spectrum of the system matrix is necessary to find appropriate parameters.

III. Application onto AlGaAs/GaAs RTDs

The most relevant structural parameters of the RTD are given in Fig. 1a. The hopping terms are calculated using $\gamma_{\text{GaAs-GaAs}} = \hbar^2/(2m_{GaAs}a_0^2)$ with $m^*_{\text{GaAs}} = 0.063 \cdot m_0$ and a similar term for $\gamma_{\text{AlGaAs-AlGaAs}}$ with $m^*_{\text{AlGaAs}} = (0.063 + 0.083x)m_0$ where x is the Al alloy content. The same expression can be used for $\gamma_{GaAs-AlGaAs}$ albeit with the harmonic mean value of the two effective masses. The onsite energies are calculated to result in conduction band energies of $E_{\text{C,GaAs}} = 1.424$ eV and $E_{\text{C,AlGaAs}} = 1.424 + d_{EC} \cdot (1.155x + 0.37x^2)$ eV with $d_{EC} = 0.73$ to account for the band offset. A constant lattice constant of $a_0 = 0.5$ nm is chosen for the sake of simplicity as it only affects the way the potential is calculated. For the source and drain regions, a doping concentration of $2{\cdot}10^{18}$ dopants $\cdot$ cm^{-1} is used with an intrinsic channel region in between, where the flatband potential is assumed to decrease linearly within.

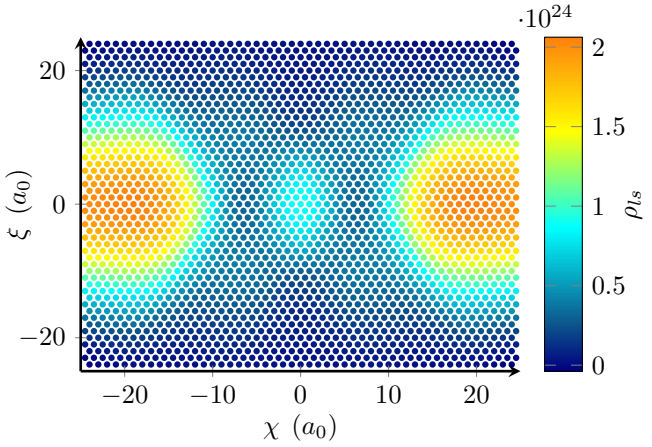

Fig. 2. Cutout of the center section of the density matrix around the barriers as calculated on a staggered grid for the equilibrium case with a constant effective mass and gallium alloy content x=0.2.

Regarding the computational domain, $N_\xi = 85$ and $N_\xi = 84$ discrete values in ξ-direction are used for the $\boldsymbol{p}$ and $\boldsymbol{q}$ grid, respectively. The number of χ values directly follows from the device length from which $N_\chi = 227$ values fall on the $\boldsymbol{p}$ grid and $N_\chi = 226$ values on the $\boldsymbol{q}$ grid. A complex absorbing potential is added to minimize reflections due to the finite computational domain [12]. The time derivative is approximated by use of a fourth order Runge-Kutta method [13] with a time step width of $2 \cdot 10^{-17}$ s.

A. Results

Part of the real space density matrix for the equilibrium case and an alloy content of $x = 0.2$ is shown in Fig. 2 as a scatter plot to further visualize the computational domain consisting of the two staggered grids. The charge carrier density for the same alloy content, spatially varying hopping terms and an applied voltage of $V_{DS} = 0.1$ V is shown in Fig. 3, along with reference results obtained by a quantum transmitting boundary method (QTBM) for the same tight-binding Hamiltonian. Even though device boundaries are treated vastly different in these two approaches, the charge carrier densities agree well. The same can be said for the drain-end current densities shown in Fig. 4 for the two different alloy contents and spatially constant, as well as varying, hopping terms. Some deviations of the drain-end current densities occur at higher applied voltages, likely from the aforementioned challenges in finding adequate inflow boundary conditions. Finally, the time-resolved evolution of the expectation values can be seen in Fig. 5 after the drain-source voltage is switched from $V_{DS} = 0.15$ V to $V_{DS} = 0.25$ at $t = 0$ s

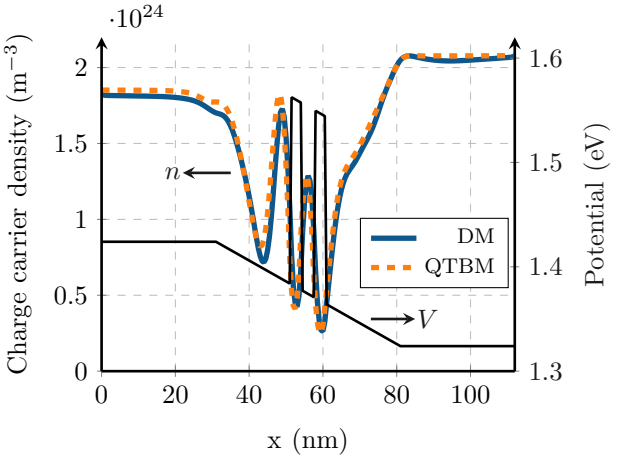

Fig. 3. The charge carrier densities from the tight-binding density matrix approach (DM) are shown for x=0.2 and spatially varying hopping terms for an applied drain-source voltage of 0.1 V, along with the flatband potential and reference results obtained by a QTBM.

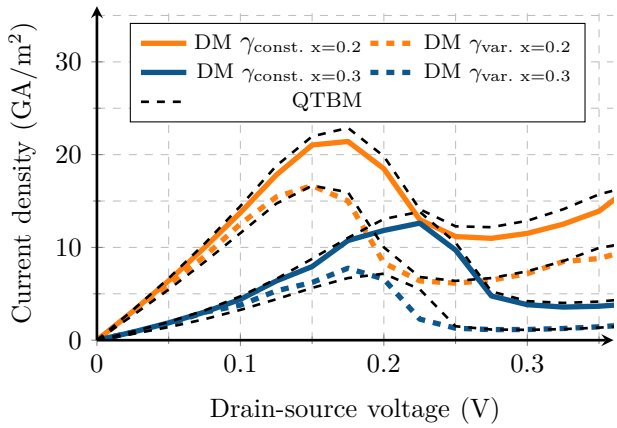

Fig. 4. The current densities from the tight-binding density matrix approach (DM) agree well with the QTBM reference results.

for $x = 0.2$ and spatially varying hopping terms. Good convergence towards the stationary current density is achieved. The inset also shows reference results obtained from a QLTE with the inclusion of a spatially varying effective mass [11]. Again, the results mostly coincide with small oscillations that can be seen for the proposed approach, likely stemming from the interaction with the device contacts.

Acknowledgment

This work was supported by the German Research Funding Association Deutsche Forschungsgemeinschaft (DFG) under Grants SCHU 1016/8 and SCHU 1016/8-3. Computing time was provided on the LiDO3 cluster, partially funded by the DFG as project 271512359

References

[1] J. Weinbub and D. K. Ferry, "Recent advances in Wigner function approaches," Applied Physics Reviews, vol. 5, no. 4, p. 041104, 10 2018.

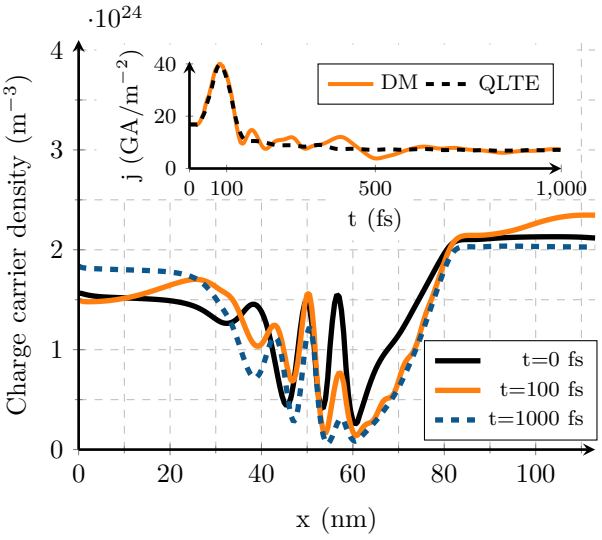

Fig. 5. The transient evolution of the drain-end current densities is shown in the inset for the DM and QLTE, along with the charge carrier densities at $t = 0$ fs, 100 fs and 1000 fs obtained by the proposed approach.

[2] Y. Xue, S. Datta, and M. A. Ratner, "First-principles based matrix green's function approach to molecular electronic devices: general formalism," Chemical Physics, vol. 281, no. 2, pp. 151–170, 2002.

[3] M. Luisier and G. Klimeck, "Atomistic full-band simulations of silicon nanowire transistors: Effects of electron-phonon scattering," Phys. Rev. B, vol. 80, p. 155430, Oct 2009.

[4] M. Pech, A. Abdi, and D. Schulz, "Time-resolved analysis of dual-gate FETs with non-parabolic energy dispersion for THz applications," Journal of Applied Physics, vol. 135, no. 7, p. 074303, 02 2024.

[5] A. Abdi, M. Pech, and D. Schulz, "Incorporation of the tight binding hamiltonian into quantum liouville-type equations," in International Workshop on Computational Nanotechnology (IWCN), 2023.

[6] C. Goringe, D. Bowler, and E. Hernandez, "Tight-binding modelling of materials," Reports on Progress in Physics, vol. 60, no. 12, p. 1447, 1997.

[7] J. Schlösser and A. Stahl, "A symmetry adapted rpa: Dynamics of the electronic density matrix in a semiconductor," physica status solidi (b), vol. 153, no. 2, pp. 773–785, 1989.

[8] R. Mains and G. Haddad, "An accurate re-formulation of the wigner function method for quantum transport modeling," Journal of Computational Physics, vol. 112, no. 1, pp. 149–161, 1994.

[9] W. R. Frensley, "Boundary conditions for open quantum systems driven far from equilibrium," Rev. Mod. Phys., vol. 62, pp. 745–791, Jul 1990.

[10] R. Kosik, J. Cervenka, and H. Kosina, "Numerical constraints and non-spatial open boundary conditions for the wigner equation," Journal of Computational Electronics, vol. 20, no. 6, pp. 2052–2061, 2021.

[11] L. Schulz, B. Inci, M. Pech, and D. Schulz, "Subdomain-based exponential integrators for quantum liouville-type equations," Journal of Computational Electronics, vol. 20, no. 6, pp. 2070–2090, 2021.

[12] L. Schulz and D. Schulz, "Complex absorbing potential formalism accounting for open boundary conditions within the wigner transport equation," IEEE Transactions on Nanotechnology, vol. 18, pp. 830–838, 2019.

[13] V. Ganiu and D. Schulz, "Discontinuous galerkin concept for quantum-liouville type equations," Solid-State Electronics, vol. 200, p. 108536, 2023.